Carbon 155 (2019) 309–319

Contents lists available at ScienceDirect

Carbon

journal homepage: www.elsevier.com/locate/carbon

Structural evolutions of small aromatic mixtures under extreme temperature conditions: Insights from ReaxFF molecular dynamics investigations

Cuiying Jian [a], Shamel Merchant [b], Xining Zang [a, ***], Nicola Ferralis [a, **], Jeffrey C. Grossman [a, *]

[a] Department of Materials Science and Engineering, Massachusetts Institute of Technology, Cambridge, MA, USA
[b] ExxonMobil Research and Engineering Co, Annandale, NJ, USA

ARTICLE INFO

Article history:
Received 24 July 2019
Received in revised form
13 August 2019
Accepted 14 August 2019
Available online 16 August 2019

ABSTRACT

Conversion mechanisms of carbonaceous materials during controlled pyrolysis under high temperature currently rely on empirical understanding, rather than a detailed atomistic description of the underlying chemical evolution. In this work, a series of molecular dynamics simulations, based on reactive force fields, were performed to probe the structural evolutions of small aromatic (number of aromatic rings $\leq$ 4) mixtures under extreme conditions (temperature 3000–4000 K). For any temperature studied and independent of the presence of alkane radicals, three major gas-phase byproducts, H_2, C_2H_2, and C_2H_4, were found in bulk treated by rapid heating. Temperatures as well as alkane addition can affect the production/consumption rates and fractionation of these gas species. Compared to alkane radicals, temperatures also play important roles in modulating the initial growth pathways of solid carbon clusters. At 3000 K, aromatic carbon cluster formation is mainly initiated through the direct combination of aryl radicals. Conversely, at 4000 K, carbon cluster formation is initiated by the assembly of chained radicals, since substantial polyacetylenic chains were produced. Through cross comparison on different simulation models/methods, as well as with experiments, the effect of processing conditions on carbonaceous materials conversion was revealed, and underlying mechanisms responsible for the observed phenomena are proposed.

1. Introduction

Industrial production of ethylene (over 150 million tons in 2017 [1]) is accompanied by the massive generation of steam cracked tar with high aromatic content [2–6]. Compounds containing one to four aromatic rings (see Fig. 1a), in addition to their natural occurrence in steam cracked tar, are also important additives required by heavy tar (rich in asphaltene and toluene insolubles) to reduce its viscosity [6]. Along with other heavy hydrocarbons (such as bitumen, vacuum residues, fuel oil, asphalthenes and other fractionated hydrocarbon streams with high boiling points) tar has been shown to be used as feedstock to create novel functional materials through controlled graphitization [7]. Annealing conversion processes involving extensive high temperature heat treatments when applied to heavy hydrocarbons are usually explained in terms of known empirical pyrolytic mechanisms. It is thus of great interest to have a detailed description of the microscopic structural evolution of aromatics under these extreme conditions. Yet, while pyrolytic reactions of each substance listed in Fig. 1 have been investigated previously (for instance, benzene [8], naphthalene [9], and pyrene [10], to list a few), a detailed distribution analysis of the final products, as well as their formation pathways, are lacking at an atomistic level, especially under the conditions of interest here.

In the last two decades, atomistic simulations, utilizing reactive force fields (ReaxFF) [11], have been widely adopted to probe the formation mechanisms of volatile gas, char, tar, soot, and layered graphene from the pyrolysis/combustion of alkanes [12–15], lignite [16,17], coal [18–20], cellulose [21], polyimides [22], polycyclic

* Corresponding author.
** Corresponding author.
*** Corresponding author.
E-mail addresses: xzang@mit.edu (X. Zang), ferralis@mit.edu (N. Ferralis), jcg@mit.edu (J.C. Grossman).

https://doi.org/10.1016/j.carbon.2019.08.048
0008-6223/

a)

Chemical Formula	Chemical Structure	Number
$C_{12}H_8S$, dibenzothiophene	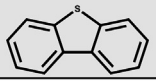	36
$C_{13}H_9N$, acridine	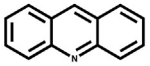	1
C_8H_9N, indoline	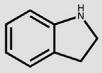	3
$C_{19}H_{14}$, 2-Methylchrysene	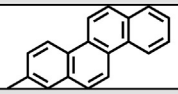	12
$C_{16}H_{10}$, pyrene		12
$C_{15}H_{12}$, 2-Methylanthracene	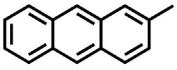	36
$C_{14}H_{10}$, phenanthrene	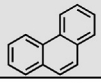	36
$C_{12}H_{10}$,biphenyl	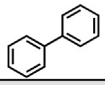	36
$C_{10}H_8$, naphthalene		36
C_9H_{10},indane		12
C_6H_6, benzene		12

b)

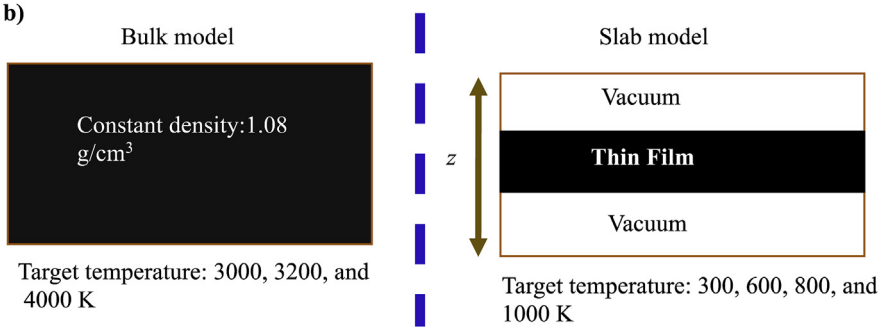

Fig. 1. a) Aromatic compounds studied in this work; **b)** the two types of simulations performed. (A colour version of this figure can be viewed online.)

aromatic hydrocarbons [23], kerogen [24], ethanol [25], and benzene [26]. For instance, it was shown that naphthalene, anthracene, and pyrene cannot grow into incipient soot particles at temperatures $\leq$ 2000 K, although at 2500 K, soot growth was observed via self-assembly of fullerene-like particles [23]. In other works, classical molecular dynamics (MD) with ReaxFF were used to show that the main byproducts (H_2O_2, H_2O, CH_2O, and CO_2) from combustion of lignite are consistent with available experimental data, and hydrogen abstraction reactions are responsible for the formation of H_2O_2 and H_2O [17]. Furthermore, ReaxFF MD with *ns* time scale was utilized to reveal reactive pathways that are compatible with the short reaction times during laser annealing (~us [27–30]); for example, the simulations predicted that a temperature > 2400 K and a pressure of ~3 GPa are necessary to crystallize layered graphene clusters from polyimides without a metal catalyst [22]. More recently, ReaxFF has been employed to investigate the effect of water on the liquefaction of lignocellulose biomass [31], the effect of nickel clusters on the formation of incipient soot particles from a single type of polycyclic aromatic hydrocarbon [32], pyrolysis of binary fuel mixtures (JP-10/toluene or n-dodecane/toluene) at supercritical conditions [33], as well as the carbonization process for C/H/O/N-based polymers [34]. Those studies demonstrate the applicability of ReaxFF based MD techniques in revealing reaction pathways at an atomistic level. Yet, most of them were confined to

systems of low aromatic content.

In this work, we employ ReaxFF-based MD simulations to probe the structural evolutions of light tar fractions (mixtures of molecules listed in Fig. 1) under high temperatures. Formation pathways of volatile byproducts were revealed, followed by kinetic descriptions and structural characterizations of solid byproducts. Cross comparisons of different simulation models/methods, as well as with experiments, were made to further validate our observations, elaborate implications, and reveal the role of processing conditions on the final products. It was found that temperature can modulate the reaction pathways of aromatics through tuning the sequence of appearance and subsequent evolution of two relevant reactions (ring opening vs. pyrolysis).

2. Simulation methods

The composition of the molecular set studied in this work is shown in Fig. 1a. As can be seen, these molecular models cover the size range of one-, two-, three- and four-ring aromatics, and structural variations include bridging, methyl substitutions, heteroatom inclusion, and presence of 5-member rings. Such molecular selection or ratio is not comprehensive, but it is representative of the broad distribution of molecular constituents in tar materials [35].

The initial configuration of each system studied was first generated by randomly packing the corresponding concentrations of molecules into a rectangular box with an initial overall density ~1 g/cm^3. Then, non-reactive dynamic equilibration was performed in the NPT ensemble at 400 K and 1 bar for 1 ns, followed by quenching to 300 K over 1 ns and re-equilibration at 300 K for 1 ns. Next, two types of systems were simulated to probe subsequent reactions: 1) bulk model (to simulate rapid heat treatment in bulk): the box dimensions were held fixed, with constant density along the simulation trajectory (left panel in Fig. 1b), and 2) slab model (to simulate rapid heat treatment at the surface): the box dimension in the z direction was expanded to introduce vacuum spaces (right panel in Fig. 1b). These systems were then gradually heated from 300 K to the target temperatures (heating rate: 0.1 K/fs), and subsequently subjected to constant temperature dynamics at the given temperature. A Nose-Hoover thermostat [36,37] was used in all constant temperature simulations.

During the non-reactive equilibration, a polymer consistent force field (PCFF) available in MedeA® [38] was chosen to describe intramolecular interactions. Non-bonded interactions were modeled using COMPASS (class 2) with long-range Coulombic interactions handled by a particle-particle particle-mesh solver [39]. After equilibrations, the reactive potentials from the work of van Duin et al. on coal [19] were adopted to describe interatomic interactions. The bond order cutoff for molecular recognition is 0.3 throughout this work, following the values reported in Refs. [17,40]. All simulations were performed using LAMMPS [41]; VMD [42] and OVITO [43] were used for visualization.

3. Results and discussion

We first focus on simulations performed on the bulk model, and the systems studied will be referred to as B3000 (temperature = 3000 K), B3200 (temperature = 3200 K), and B4000 (temperature = 4000 K). Since alkanes might be present in tar due to incomplete cracking [2–6], one additional simulation was performed to probe the effect of octane (~6.67 wt%) at 4000 K (denoted as system BO4000). For each system, the results were averaged over three independent runs.

3.1. Gas-phase byproducts in bulk

Fig. 2 shows the gas-phase byproducts (defined as molecules

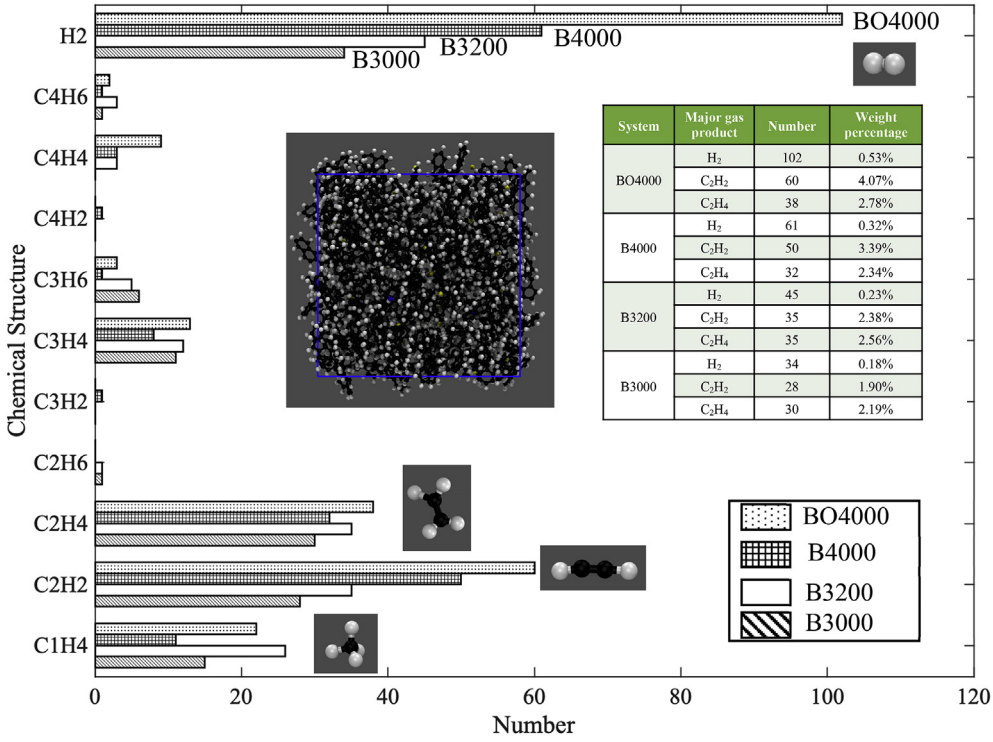

System	Major gas product	Number	Weight percentage
BO4000	H_2	102	0.53%
	C_2H_2	60	4.07%
	C_2H_4	38	2.78%
B4000	H_2	61	0.32%
	C_2H_2	50	3.39%
	C_2H_4	32	2.34%
B3200	H_2	45	0.23%
	C_2H_2	35	2.38%
	C_2H_4	35	2.56%
B3000	H_2	34	0.18%
	C_2H_2	28	1.90%
	C_2H_4	30	2.19%

Fig. 2. Gas byproducts at the end of the simulation in systems B3000, B3200, B4000, and BO4000: the inset table shows the absolute number and weight percentage of the three major gas species. For clarity, bars are labeled in one example (see H_2); the order of bars is the same for each chemical structure. (A colour version of this figure can be viewed online.)

with number of carbon atoms ≤ 4, threshold chosen based on previous work [40,44]) obtained at the end of the different simulations (for the attainment of dynamic equilibrium, i.e., product distribution remaining unchanged, see Supplementary Data, section S1). The three major gas-phase byproducts were found to be H_2, C_2H_4, and C_2H_2 (shown in the inset table of Fig. 2), regardless of the simulated temperatures and molecular concentrations.

Detailed examination of Fig. 2 shows that H_2 appears as the most abundant species in terms of the number of gas-phase molecules in each system, and the absolute amount of each species can be system-dependent. Clearly, both increasing temperature and the inclusion of octane enhance the net H_2 and C_2H_2 production while their effects on the production of C_2H_4 is limited. The increase of H_2 can be attributed to the enhanced dehydrogenation in the case of increased temperature; on the other hand in system BO4000, the increase in H_2 product is the result of an overall increased H/C ratio in the original reactants [13]. To further explore the reaction kinetics of C_2H_2 and C_2H_4, Figs. 3 and 4 show their production/consumption rates/channels in systems B3000, B4000, and BO4000.

First, the legend in Fig. 3a lists all possible channels: H + C_2H, 2CH, and C_2H_2, where the subscript indicates the number of carbon or hydrogen atoms involved. These three channels correspond to a combination of one H radical and one C_2H radical, a combination of two CH radicals, and a direct formation from cracking in producing C_2H_2, and indicate a decomposition of acetylene into one H radical and one C_2H radical, a decomposition into two CH radicals, and a direct addition of acetylene to other substances in consuming C_2H_2. These channels were determined by first identifying the C_2H_2 molecules newly formed at time t compared to those at time t-Δt (Δt = 15 ps for system B3000). For each newly formed molecule, the atoms involved were further analyzed to determine which molecules they belonged to at time t- Δt For instance, if atom H in a particular newly formed C_2H_2 molecule at t = 287 ps belong to molecule A at t = 272 ps, and the other three atoms C_2H all belongs to molecule B at t = 272 ps, this C_2H_2 molecule was categorized to

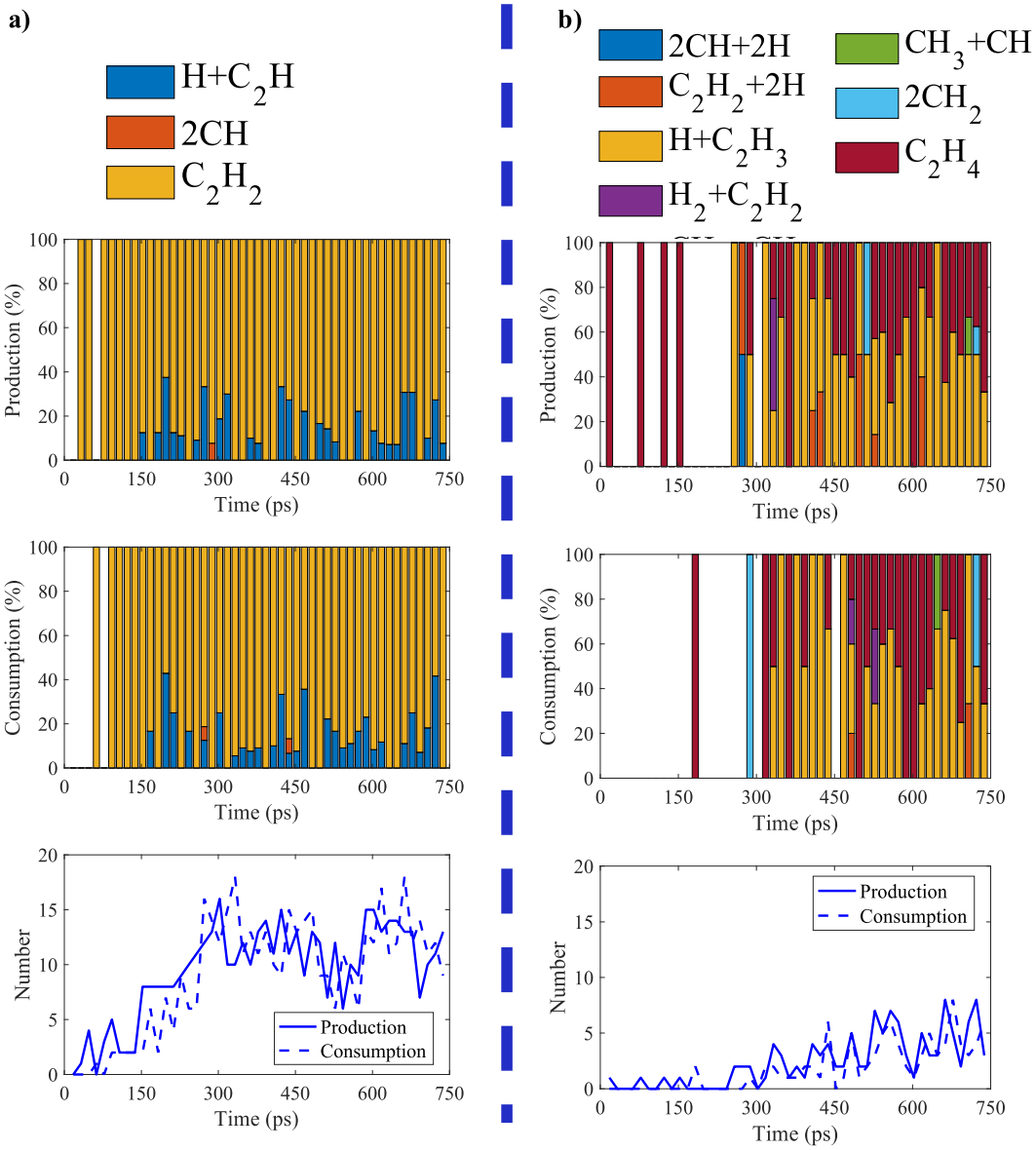

Fig. 3. **a)** C_2H_2 and **b)** C_2H_4 production/consumption in system B3000. In both subfigures, the top panel depicts production, the middle panel indicates consumption, and the bottom panel plots number counts of production/consumption. (A colour version of this figure can be viewed online.)

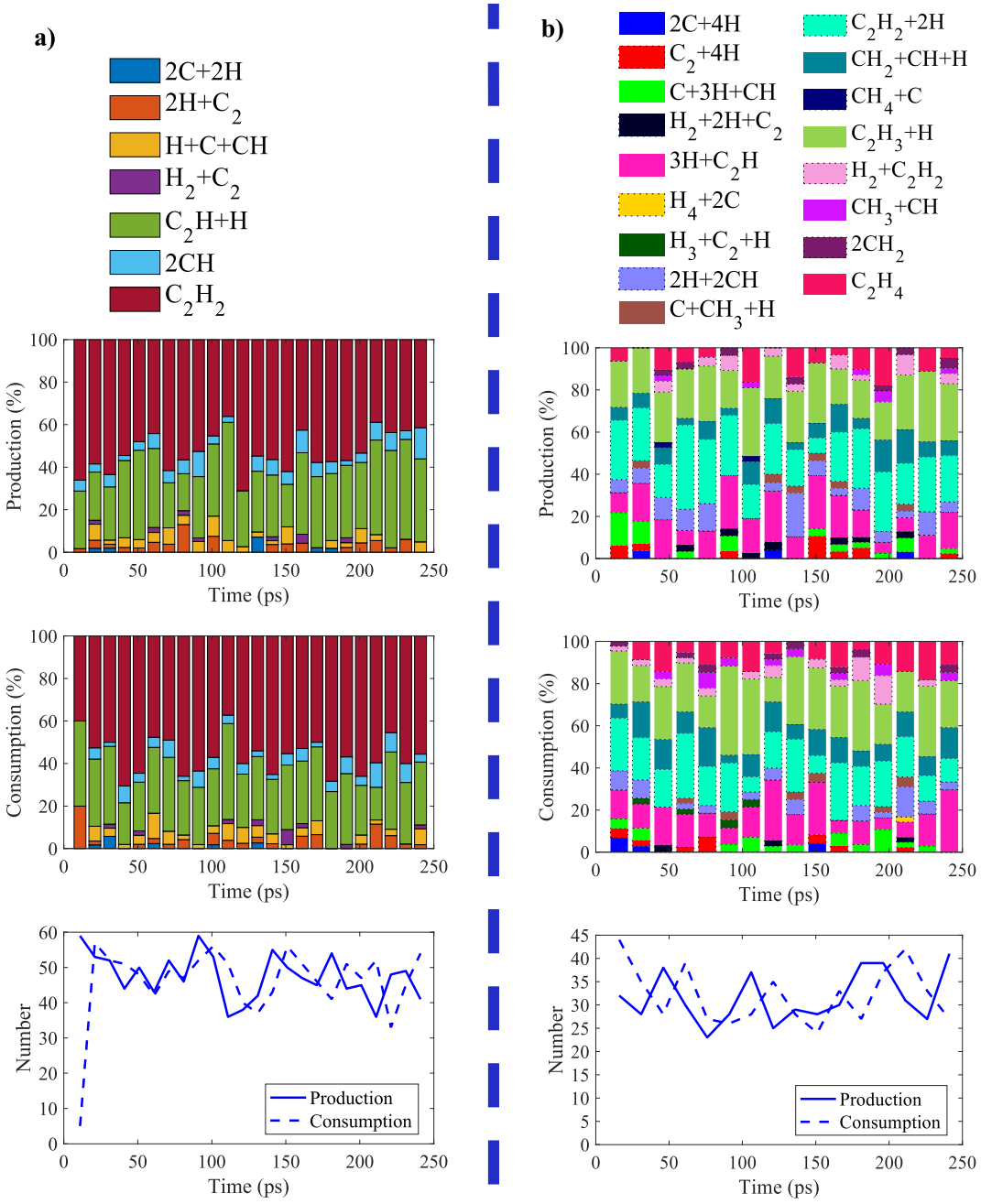

Fig. 4. **a**) C_2H_2 production/consumption in system B4000, and **b)** C_2H_4 production/consumption in system BO4000. In each subfigure, the top panel depicts production, the middle panel indicates consumption, and the bottom panel plots number counts of production/consumption. (A colour version of this figure can be viewed online.)

be formed through a combination channel of H + C_2H. By looping through all newly formed C_2H_2 molecules, the percentage of each channel in generating C_2H_2 at $t = 287$ ps can be determined, and it is summarized in the top panel of Fig. 3a. We note that following this method, unusual species, such as C, CH, and C_2, might present in reaction channels, which indicates that in forming C_2H_2, reactant molecules at time t-Δt supplied a single C atom, CH or C_2. Furthermore, the reaction events summarized represent all possible production pathways at these high temperatures. We do not intentionally filter out any reactions or apply a hidden Markov model to distinguish different reactions, since all the information is embedded in the percentage distribution presented here. Similarly, consumption channels/reactions can be determined (middle panel in Fig. 3b).

Detailed examination of Fig. 3a (system B3000, temperature = 3000K) shows the major production channel of C_2H_2 is direct cracking, accounting for 100% before ~135 ps, and over 50% for the remaining simulation time (750 ps). Major consumption channels are the reverse reactions of the production channels. Furthermore, both the production and consumption number count of C_2H_2 exhibit an increasing trend up to ~300 ps with a final value ~12 (for representative net number, see Supplementary Data, section S2).

As for the production of C_2H_4 in system B3000 (Fig. 3b), the dominating role of direct cracking in production is not as significant as that for C_2H_2. Specifically, starting from ~255 ps, the combined production channel of H and C_2H_3 emerges as one of the major

production channels, accounting for 100% of the production during certain parts of the simulation. Other production channels are also found to be important including 2CH+2H, C_2H_2+2H, H_2+C_2H_2, and $2CH_2$, each of which was shown to account for up to ~50% of the production at various points in the simulations (after 250 ps). Generally, reverse reactions of major production channels are the main channels for consumption. The production/consumption of C_2H_4 heavily involves other radicals compared to the channels of C_2H_2, which can explain its smaller number counts (bottom panels in Fig. 3b). The difference between C_2H_4 and C_2H_2 is consistent with previous findings that H- and C_2H_2-loss possesses the lowest energy channels during the pyrolysis of aromatics [23,45].

For system B4000 (Fig. 4a), the production channels of C_2H_2 are more diverse compared to those in system B3000 (Fig. 3a), and the dominant role of direct cracking in producing C_2H_2 is absent here, with only ~50% of C_2H_2 produced from direct cracking. The second major production channel involves a combination of C_2H and H, and accounts for ~30% of C_2H_2 production. Similarly, consumption channels are again more diverse in system B4000 than those in system B3000. Regarding the number counts, the C_2H_2 production number count is ~60 as soon as the constant heating stage starts in system B4000, and the consumption number count reaches ~50 within ~20 ps of the simulation time. Comparing with the gradual increase in system B3000, these observations suggest rapid reaction kinetics at a higher temperature (4000 K). For C_2H_4 (see Supplementary Data, section S3), again, the major differences between the results for the simulations at these two temperatures lie in the increased rates and more diverse channels available at 4000 K. For example, unlike the case at temperature = 3000 K, direct cracking and a combination of H + C_2H_3 dominates the production with overall number count less than 10, at temperature = 4000 K, an additional channel (a combination of 2H + C_2H_2) appears with total number count ~20 at later stages of the simulation.

When considering system BO4000 (Fig. 4b), the percentage of direct cracking in producing C_2H_4 is further decreased, and the other three most important production/consumption channels were found to be C_2H_3+H, C_2H_2+2H, and 3H + C_2H. More interestingly, C_2H_4 production/consumption number counts are ~40 as soon as the constant heating stage starts, mainly a result of the decomposition of octane during the heating up stages (see Supplementary Data, section S4). As the aromatics begin to crack during the constant heating stage, production/consumption channels of C_2H_4 become more diversified. Overall, the highest number counts of C_2H_4 production/consumption are observed here among the three systems considered, and similar effects were observed for C_2H_2 (see Supplementary Data, section S3).

From these results, gas byproduct production/consumption rates and channels are mainly determined by both temperature and the presence of octane, which in turn might lead to different consumption rates/pathways of the reactants and result in different formation mechanisms of solid carbon clusters. For instance, the drastic cracking of aromatics induced at 4000 K may lead to massive formation of polyacetylenic chains as suggested in the work of Mao et al. [23] Therefore, in the following section we present a detailed characterization of the evolution of solid structures (carbon clusters).

3.2. Solid fraction formation

Fig. 5a and b depict the growth of representative carbon clusters during the simulations in systems B3000 and B4000. These plots show the bonding connectivity among atoms, and do not contain the actual coordinate information. At 3000 K, aryl radicals, formed by H- or C_2H_2 loss, can directly interconnect through bond formation between carbon atoms. This clustering can lead to the formation of molecules with more than 4 rings (maximum no. of rings in the reactant molecules is 4, see Fig. 1a). For instance, at 10 ps, the molecule shown contains 6 rings. This growth pathway shares significant similarities with soot particle inception through polymerization of polyaromatic hydrocarbons [46]. Conversely, at temperature of 4000 K, carbon clusters (Fig. 5b) contain significant fractions of polyacetylenic chains (indicated by arrows in Fig. 5b), which act as linkers between adjacent aromatic regions. These polyacetylenic chains result from the massive ring opening at the initial stage (as early as 0.1 ps). This growth pathway resembles soot particle inception involving the assembly of polyacetylenic chains [23].

In order to understand the evolution of rings at 3000 K and 4000 K, 6-member and 5-member rings are tracked in Fig. 6, since they are present in the original reactants (Fig. 1a). Rings that are from reactants and remain intact during pyrolysis are denoted using “original” in the legend; in contrast, “total” counts all the rings present in the system including rings that remained intact as well as rings newly formed. At both temperatures, the number of original rings decays due to ring opening as well as forming radical byproducts, and the decaying rates depend strongly on

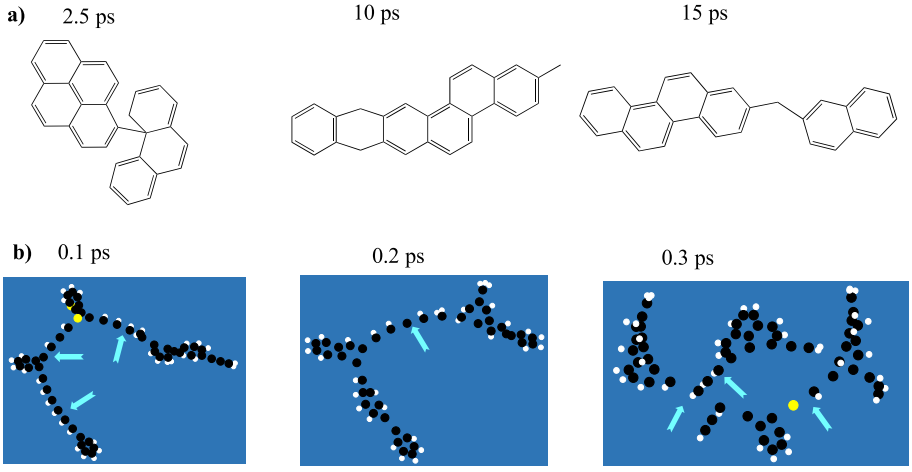

Fig. 5. Initial growth pathway of representative carbon clusters in systems **a)** B3000 and **b)** B4000. Given the different reaction kinetics, in a), the growth pathway was illustrated using chemical structures; in **b)**, lines denote bonds, and balls represents atoms, among which black represents carbon, yellow denotes sulfur, and white indicates hydrogen. Arrows in b) indicate the formation of polyacetylenic chains. (A colour version of this figure can be viewed online.)

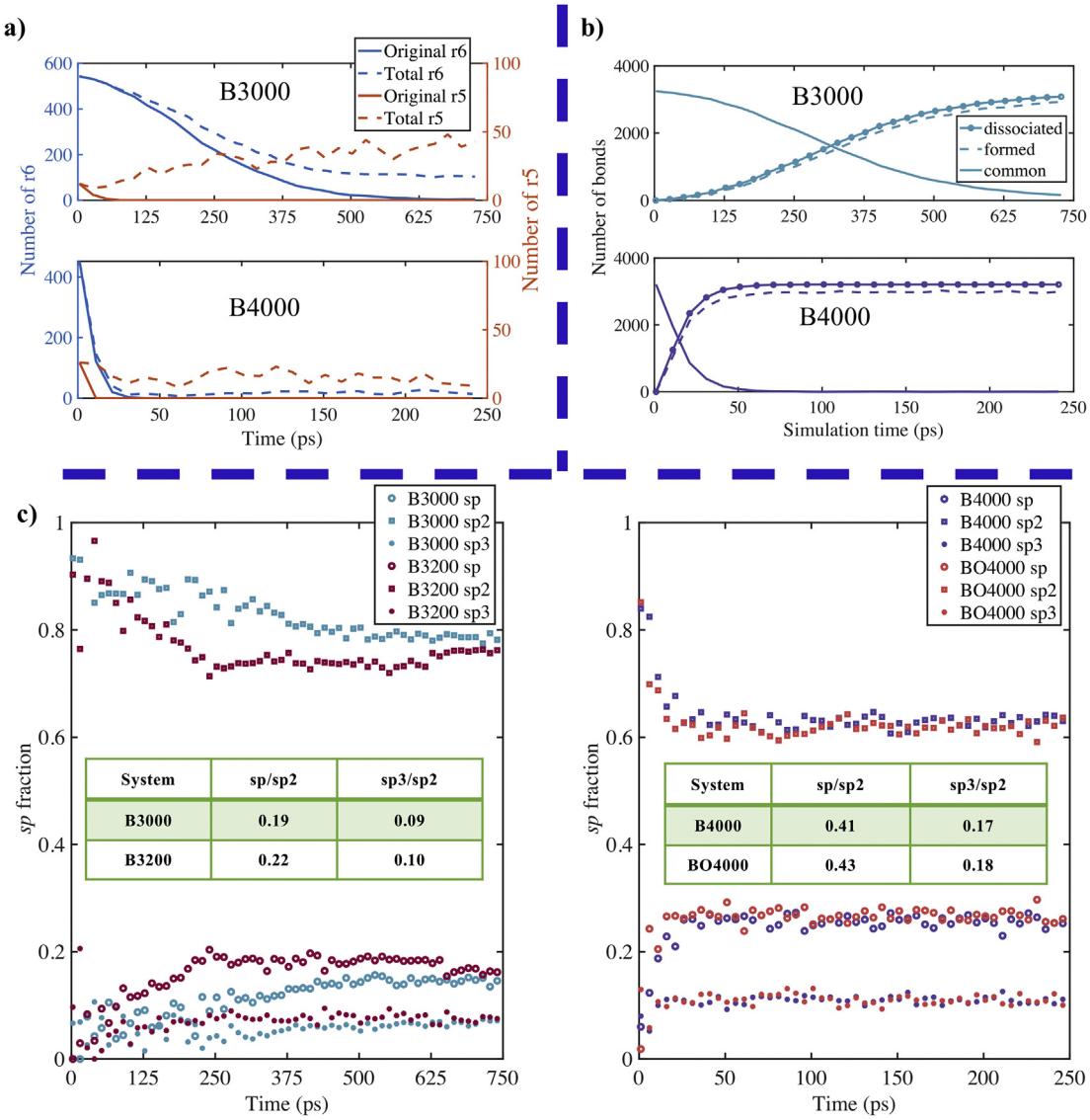

Fig. 6. a) number of 6-member (r6) rings (right axis) and 5-member (r5) rings (left axis), **b)** number of bonds, and **c)** *sp* fraction. All are plotted as a function of simulation time. (A colour version of this figure can be viewed online.)

temperature, confirming the different kinetics shown in Fig. 5. Further examination of Fig. 6a shows the formation of new 5-member and 6-member rings at temperature = 3000 K, evidenced by the vertical gap between the "original" and "total" curves, while at temperature = 4000 K, new ring formation is much less frequent, indicated by the near overlapping of the "original" and "total" curves. The overall decrease of 6-member rings observed here is consistent with previous findings on benzene reactions [47,48], where combustion was mimicked by hydrogen removal, as well that in the work of Kowalik et al. [34], which reported a delay in the 6-membered ring productions for the carbonization of poly(*p*-phenylene-2,6-benzobisoxazole) with relatively lower aromatic content.

At both temperatures (3000 K and 4000 K), the final number of original 6/5-member rings decays to ~0, suggesting that all original bonds can be dissociated. In Fig. 6b, taking the initial bonding network as a reference, dissociated bonds represent original carbon-carbon bonds that have been broken, formed bonds represent new carbon-carbon bonds that do not initially exist, and common bonds represent original carbon-carbon bonds that remain unchanged. In all cases, the number of common bonds decay to ~0, and the lines representing newly formed bonds nearly overlap with those of dissociated bonds. In essence, almost all products (gas or solid), regardless of the formation pathways, undergo mass exchange with their surrounding environment. These results are in agreement with previous works showing that small aromatics similar to the ones studied here cannot survive at a temperature $\geq$ 2400 K [23]. Their decomposition and fragmentation are substantial as constant heating continues [23], and can be further accelerated by the presence of nickel clusters [32].

At both temperatures (3000 K and 4000 K), the different number of total 6/5-member rings indicate different aromatic contents, and hence different hybridization fractions. To confirm this, the *sp* fraction is plotted as a function of simulation time for systems B3000, B4000, B3200 and BO4000 in Fig. 6c. In general, sp^2 fraction decreases with time in all four systems, accompanied by an increasing trend of *sp* and sp^3, especially *sp* fractions, suggesting that while different growth pathways were observed initially, ring opening, and thus the formation of polyacetylenic chains, is evident in the later stages of all simulations. The *sp* fractions reach steady

values, respectively, at ~10 ps in system B4000 and ~300 ps in systems B3000, reflecting the elevated reaction kinetics of higher temperature (4000 K). More importantly, when the temperature reaches 4000 K, the equilibrium value of sp^2 fraction is decreased, with increased *sp* and sp^3 fractions, leading to increased sp/sp^2 and sp^3/sp^2 ratios (see the inset tables in Fig. 6c). That is, starting from a very high aromatic content (sp^2 fraction accounts for ~100% of the original reactants), high temperature would lead to a decrease in aromatic content. We note that given its relatively low concentration (~6.67 wt%), the presence of octane does not impact the *sp* fractions, suggesting the dominant role of aromatics. These results are consistent with literature works reported on benzene reactions (Fig. 3 of Ref [47] and Fig. 5a of Ref [48], before hydrogen removal).

The above discussion can thus help in elucidating the solid growth pathways at these two temperatures. At 3000 K, the evolution of the solid portion is initiated by the polymerization of reactants, and as the simulations further proceed, ring opening starts to appear, leading to the formation of polyacetylenic chains. The assemblies of these polyacetylenic chains help connect the aromatic regions (either newly formed or reserved from original reactants, Fig. 5a). On the other hand, at 4000 K, given the elevated reaction rate, the formation of poyacetylenic chains is evident as soon as the simulation starts, and the interconnection of polyacetylenic chains, consisting of ~3–7 carbon atoms, dominates the solid formation pathway. At both temperatures, solid particles undergo constant mass exchange with the surrounding environment. Regarding the final solid structures (carbon cluster), lower temperature (3000 K) introduces a higher aromatic content as well as *sp2* fraction compared with higher temperature (4000 K).

3.3. Discussions and implications

Given that the above results were obtained from simulations performed on bulk models in the NVT ensemble, we note that a pressure of ~1–3 GPa was generated at the constant heating stage. This high pressure might be partially attributed to the accelerated kinetics of gas byproducts, despite that they only account for <10% of reactant mass. For instance, the diffusion coefficient of hydrogen gas in our system is ~ $10^{-4} cm^2/s$ at 3000 K, consistent with the values reported for hydrogen diffusion in pyrolytic carbon, and orders of magnitude higher than that at 300 K as described by an Arrhenius relation [49]. To demonstrate that these high pressures are necessary for the formation of solid clusters, we performed a series of simulations using the slab model (right panel in Fig. 1b, reference pressure ~0), and the relevant results are summarized in Fig. 7.

As can be seen, for the slab model, an evident increase in both the total number of molecules (Fig. 7a) and the total number of species (Fig. 7b) is observed at a temperature as low as 800 K. On the one hand, these increments result from the decomposition of original reactants into small molecules; on the other hand, they indicate the absence of solid products, since the formation of large carbon clusters would lead to an overall reduction in the total number of molecules. Furthermore, slab models also possess strong physical instability due to the lack of adequate pressure, which can be verified by plotting the distribution of the number of atoms along *z* axis (Fig. 7c). Clearly, compared to the initial distribution (top panel of Fig. 7c), near the end of a 500 ps simulation (bottom panel of Fig. 7c), the number of atoms left in the film, i.e., total counts in condensed phase, is negligible at 1000 K. That is, almost all atoms sublimate into gas-phase by the end of the simulation. Thus, further increasing temperature (i.e., to 3000 K or even higher) would further enhance the decomposition rate and physical instability of the slab model. We note that similar results were obtained with the slab simulations at 1000 K with the box size

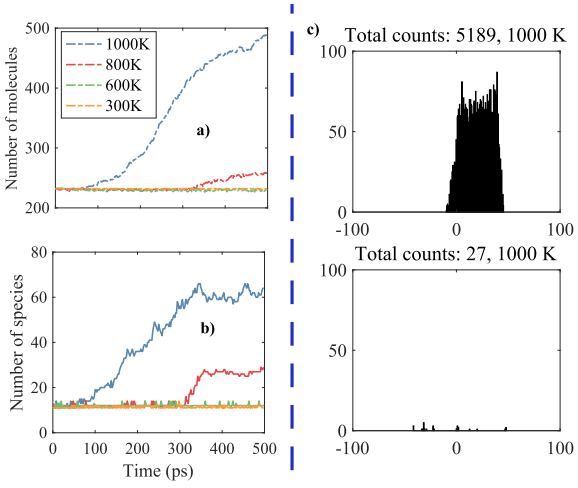

Fig. 7. Slab systems studied at 300 K, 600 K, 800 K, and 1000 K: **a)** number of molecules and **b)** number of species as a function of simulation time, and **c)** number of atoms distribution along *z* axis: initial counts (top panel), and final counts (bottom) at 1000 K. (A colour version of this figure can be viewed online.)

increased tenfold.

The observations above clearly demonstrate the critical importance of pressure during heat treatments. Depending on the time scales in experiments, gas-phase byproducts generated in bulk might be able to diffuse into the surrounding environments. In particular, these gas byproducts are hydrogen rich (Fig. 2), which has been reported to inhibit ring condensation from small aromatic molecules [9,50,51]. To probe the effects of gas removal (mainly hydrogen removal) and meanwhile keeping a condensed phase, we adopted the approach proposed in Refs. [47,48,50] where hydrogen atoms were manually removed from the reactants, and performed two additional simulations using the bulk model at 2000 K and 3500 K. The temperatures were carefully chosen to make sure they fall into the ones used in Refs. [47,48] for comparison. The final *sp* fractions for these systems are shown in Fig. 8a. The sp/sp^2 and sp^3/sp^2 ratios show, respectively, an increasing and decreasing trend from 2000 K to 3500 K, consistent with those reported in Fig. 3 of Ref [47] and Fig. 5a of Ref [48] after hydrogen removal. This was directly verified and validated experimentally, by measuring the sp^3/sp^2 fraction of a specific tar sample before and after heat treatment (done by CO_2 laser ablation in ambient air) using X-ray photoelectron spectroscopy (see Supplementary Data, section S5). With increasing power (directly proportional to temperature), the sp^3/sp^2 ratio shows a decreasing trend.

The dominant role of the sp^2 bonding environment indicates drastic ring condensation at a later stage as shown in Fig. 8b, where the total number of 6-member rings exhibits an initial decrease trend followed by an increase trend, suggesting a re-organization process of carbon atoms after the initial decomposition [22]. As for the 5-member rings, they are of critical importance for the bending of ring regions in the carbon cluster [52]. Furthermore, at a higher temperature (3500 K), layered graphitic structures were observed (stacking directions indicated by arrows in Fig. 8c), similar to the work of Dong et al. [22] where the reactants are of a much lower hydrogen to carbon ratio (~0.55). Eliminating the inhibiting effect of hydrogen, carbon clustering in the form of aromatic rings is much more favored, consistent with literature reports on fullerene formation from naphthalene, toluene, and benzene [9,50,51].

Finally, we compared the appearance and evolution of the two relevant reactions (ring opening, RO, vs. pyrolysis, PF) for all the aromatics studied in systems B3000 and B4000 (Table 1). At both

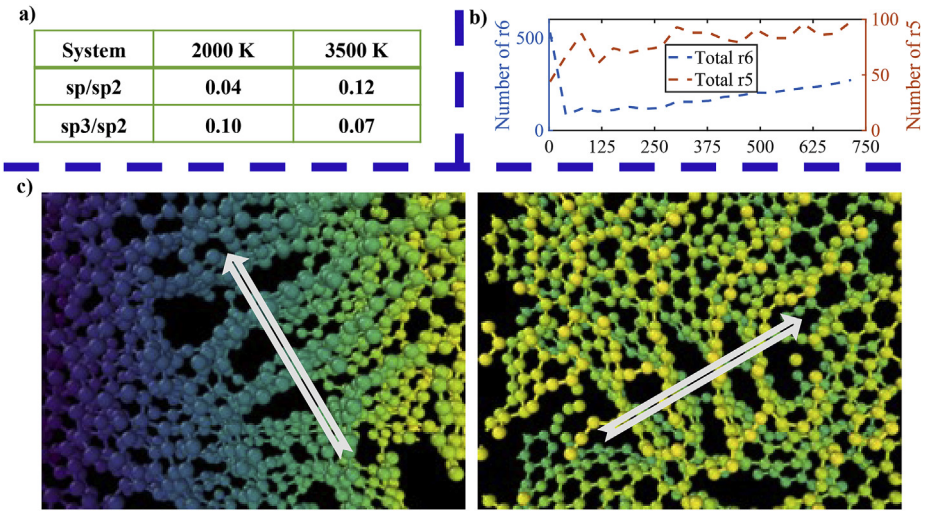

Fig. 8. a) *sp* fractions of the two additional systems with hydrogen manually removed (see main text for details); **b)** number of rings for system simulated at 2000 K; **c)** layered graphitic structures (stacking directions indicated by arrows) observed in system simulated at 3500 K. (A colour version of this figure can be viewed online.)

Table 1
Reaction (ring opening vs. pyrolysis) sequences of all reactants.

Name	4000 K RO	4000 K PF	3000 K RO	3000 K PF
$C_{12}H_8S$, dibenzothiophene	20	9	31	4
$C_{13}H_9N$, acridine	1	0	1	0
C_8H_9N, indoline	0	0	2	1
$C_{19}H_{14}$, 2-Methylchrysene	3	8	4	8
$C_{16}H_{10}$, pyrene	6	6	8	4
$C_{15}H_{12}$, 2-Methylanthracene	8	19	10	25
$C_{14}H_{10}$, phenanthrene	22	9	14	18
$C_{12}H_{10}$,biphenyl	20	11	17	16
$C_{10}H_8$, naphthalene	21	12	20	13
C_9H_{10}, indane	0	0	9	1
C_6H_6, benzene	5	7	5	7

temperatures (3000 K and 4000 K), for aromatics with heteroatoms or 5-member rings, the integrity of the molecule was first altered by ring opening. For molecules containing only 6-member rings, aromatics with 2 (naphthalene and biphenyl) or 3 rings (phenanthrene) were more prone to ring opening at 4000 K, while naphthalene was also sensitive to ring opening at 3000 K. Not surprisingly, among all the aromatics studied, only molecules with methyl groups (2-Methylchrysene and 2-Methylanthracene), were altered initially by pyrolysis. Considering the growth pathway of the carbon clusters at 3000 K and 4000 K (Fig. 5), ring opening at 3000 K would occur at a lower rate compared to that at 4000 K. Nevertheless, over the entire simulation, ring opening is evident, and responsible for the increased sp and sp3 fractions over the entire simulation course observed at 3000 K. Furthermore, different molecular structures also affect the reaction rate (see Supplementary Data, section S6). In general, aromatics with 2 or 3-rings per molecule (linear shapes) react at a higher rate than those with 1 or 4-rings (circular shapes), indicating that molecular shape/sizes could affect reaction rate as predicted using molecular orbital theory [53]. Furthermore, the presence of heteroatoms/methyl-groups/5-member rings can increase the reaction rate. In the recent work of Ashraf et al. [33], it was proposed that in mixed reactants, the pyrolysis products of reactive compounds could help less reactive molecules to decompose by lowering the activation energy of these less reactive molecules. For the aromatics studied in our work, the synergistic effects of their different reaction dynamics lead to the gas and solid production pathways observed in sections 3.1 and 3.2, which could be different from that of a single type of molecules at these temperatures. For instance, at 3000 K, relatively more reactive aromatics with 2 or 3 rings can promote solid carbon cluster formation through polymerization of reactants as early as within ~25 ps, which may not be readily observable in a system with, for instance, only benzene (stable up to ~350 ps, see Fig. s7 in Supplementary Data) present.

Taking all of our results together, we propose the following guidelines related to carbonacoues materials processing temperature conditions in the thousands of K: 1) For cracking aromatics into small molecules (no. of carbon atoms ≤ 4), initial reaction pressure should be set as small as possible. 2) For producing large carbon clusters, relatively high pressure should be maintained. In this case, if the objective is to produce carbon clusters of interconnected aromatic regions, relatively lower temperature is preferred to slow down reaction kinetics; if the objective is to increase sp or sp3 fractions, relatively high temperature is preferred to facilitate dehydration of the aromatics. 3) For producing structures of condensed rings from small aromatic molecules (similar to the ones studied in this work), the removal of gas byproducts, while maintaining a condensed phase is recommended.

4. Conclusions

In this work, we performed extensive ReaxFF-based molecular dynamics simulations to probe structural evolutions of small aromatic mixtures (number of aromatic rings ≤ 4). It was found that temperatures as well as the addition of alkanes can increase production/consumption counts of gas-phase C_2H_2 and C_2H_4, and diversify the corresponding production/consumption channels. At both temperatures (3000 K and 4000 K) studied here, the production of C_2H_4 heavily relies on other radicals, and thus, in the absence of alkanes, falls behind that of C_2H_2 which is mainly formed by direct cracking of aromatic molecules. As for the solid products, it was found that at 3000 K, carbon cluster formation is mainly initiated through the direct combination of aryl radicals; in contrast, at 4000 K, carbon cluster formation is initiated by the assembly of chained radicals. However, at both temperatures, the final solid products are of reduced sp^2 fraction, as well as reduced number of rings, compared to the original reactants. Additional simulations confirmed the importance of pressure for solid carbon cluster formation, and verified the inhibiting effect of hydrogen on ring condensation from small aromatic molecules. Overall, the

carbon cluster evolution observed at 3000 K and 4000 K is proposed to originate from the fact that aromatic molecules are more prone to ring opening than pyrolysis under the conditions studied here. These results shed light on aromatic conversion pathways under extreme conditions at an atomistic level.

Acknowledgements

We acknowledge the computing resources from the National Energy Research Scientific Computing Center, and helpful discussions with Taishan Zhu, Mark Disko, and Heather Elsen. Financial support for this research from Department of Energy and Exxon-Mobil under the MIT Energy Initiative (Grant EM09079) is gratefully acknowledged. C. J. acknowledges financial support from the Natural Sciences and Engineering Research Council of Canada Postdoctoral Fellowship.

Appendix A. Supplementary data

Supplementary data to this article can be found online at https://doi.org/10.1016/j.carbon.2019.08.048.

References

[1] Ethylene Global Supply Demand Analytics Service | Wood Mackenzie, (n.d.). https://www.woodmac.com/news/editorial/ethylene-global-supply-demand-analytics-service/(accessed March 26, 2019).
[2] S.F. Roca, R. Cited, (12) United States Patent, 2 (2006). doi:10.1038/incomms1464.
[3] US8709233B2.pdf, (n.d.).
[4] US20080099371A1.pdf, (n.d.).
[5] US20090057200A1.pdf, (n.d.).
[6] A. King, I. Robert, D. Strack, R.C. Stell, J.R. Messinger, T.X. Us, D.C. Grenoble, (12) United States Patent, 2 (2012).
[7] H.A.E. Owen P. Morris, Xining Zang, Aoife Gregg, Brent Keller, J.C.G. Mark M. Disko, Nicola Ferralis, Steam cracker tar: negative cost feedstock for transparent joule heaters, Adv. Mater. (2019), 1900331.
[8] C. Saggese, A. Frassoldati, A. Cuoci, T. Faravelli, E. Ranzi, A wide range kinetic modeling study of pyrolysis and oxidation of benzene, Combust. Flame 160 (2013) 1168–1190, https://doi.org/10.1016/j.combustflame.2013.02.013.
[9] R. Taylor, G.J. Langley, H.W. Kroto, D.R.M. Walton, Formation of C60 by pyrolysis of naphthalene, Nature 366 (1993) 728–731, https://doi.org/10.1038/366728a0.
[10] J. Mukherjee, A.F. Sarofim, J.P. Longwell, Polycyclic aromatic hydrocarbons from the high-temperature pyrolysis of pyrene, Combust. Flame 96 (1994) 191–200, https://doi.org/10.1016/0010-2180(94)90008-6.
[11] A.C.T. Van Duin, S. Dasgupta, F. Lorant, W.A. Goddard, ReaxFF: a reactive force field for hydrocarbons, J. Phys. Chem. A 105 (2001) 9396–9409.
[12] Q.-D. Wang, X.-X. Hua, X.-M. Cheng, J.-Q. Li, X.-Y. Li, Effects of fuel additives on the thermal cracking of *n* -decane from reactive molecular dynamics, J. Phys. Chem. A 116 (2012) 3794–3801, https://doi.org/10.1021/jp300059a.
[13] F. Castro-Marcano, A.C.T. van Duin, Comparison of thermal and catalytic cracking of 1-heptene from ReaxFF reactive molecular dynamics simulations, Combust. Flame 160 (2013) 766–775, https://doi.org/10.1016/J.COMBUSTFLAME.2012.12.007.
[14] X. Liu, X. Li, J. Liu, Z. Wang, B. Kong, X. Gong, X. Yang, W. Lin, L. Guo, Study of high density polyethylene (HDPE) pyrolysis with reactive molecular dynamics, Polym. Degrad. Stab. 104 (2014) 62–70, https://doi.org/10.1016/J.POLYMDEGRADSTAB.2014.03.022.
[15] Y. Liu, J. Ding, K.-L. Han, Molecular dynamics simulation of the high-temperature pyrolysis of methylcyclohexane, Fuel 217 (2018) 185–192, https://doi.org/10.1016/J.FUEL.2017.12.055.
[16] X. Guo, Z. Liu, Q. Liu, L. Shi, Modeling of kraft lignin pyrolysis based on bond dissociation and fragments coupling, Fuel Process. Technol. 135 (2015) 133–149, https://doi.org/10.1016/J.FUPROC.2014.12.009.
[17] B. Chen, Z. Diao, H. Lu, Using the ReaxFF reactive force field for molecular dynamics simulations of the spontaneous combustion of lignite with the Hatcher lignite model, Fuel 116 (2014) 7–13, https://doi.org/10.1016/J.FUEL.2013.07.113.
[18] J.-H. Zhan, R. Wu, X. Liu, S. Gao, G. Xu, Preliminary understanding of initial reaction process for subbituminous coal pyrolysis with molecular dynamics simulation, Fuel 134 (2014) 283–292, https://doi.org/10.1016/J.FUEL.2014.06.005.
[19] F. Castro-Marcano, A.M. Kamat, M.F. Russo, A.C.T. van Duin, J.P. Mathews, Combustion of an Illinois No. 6 coal char simulated using an atomistic char representation and the ReaxFF reactive force field, Combust. Flame 159 (2012) 1272–1285.
[20] J. Zhang, X. Weng, Y. Han, W. Li, J. Cheng, Z. Gan, J. Gu, The effect of supercritical water on coal pyrolysis and hydrogen production: a combined ReaxFF and DFT study, Fuel 108 (2013) 682–690, https://doi.org/10.1016/J.FUEL.2013.01.064.
[21] M. Zheng, Z. Wang, X. Li, X. Qiao, W. Song, L. Guo, Initial reaction mechanisms of cellulose pyrolysis revealed by ReaxFF molecular dynamics, Fuel 177 (2016) 130–141, https://doi.org/10.1016/J.FUEL.2016.03.008.
[22] Y. Dong, S.C. Rismiller, J. Lin, Molecular dynamic simulation of layered graphene clusters formation from polyimides under extreme conditions, Carbon 104 (2016) 47–55, https://doi.org/10.1016/J.CARBON.2016.03.050.
[23] Q. Mao, A.C.T. van Duin, K.H. Luo, Formation of incipient soot particles from polycyclic aromatic hydrocarbons: a ReaxFF molecular dynamics study, Carbon 121 (2017) 380–388, https://doi.org/10.1016/J.CARBON.2017.06.009.
[24] Y. Qian, J.-H. Zhan, D. Lai, M. Li, X. Liu, G. Xu, Primary understanding of non-isothermal pyrolysis behavior for oil shale kerogen using reactive molecular dynamics simulation, Int. J. Hydrogen Energy 41 (2016) 12093–12100, https://doi.org/10.1016/J.IJHYDENE.2016.05.106.
[25] M. Feng, X.Z. Jiang, W. Zeng, K.H. Luo, P. Hellier, Ethanol oxidation with high water content: a reactive molecular dynamics simulation study, Fuel 235 (2019) 515–521, https://doi.org/10.1016/J.FUEL.2018.08.040.
[26] X. Dong, X. Fan, Y. Fan, Y. Wen, Reactive molecular dynamics simulation of the pyrolysis and combustion of benzene: ultrahigh temperature and oxygen-induced enhancement of initiation pathways and their effect on carbon black generation, RSC Adv. 5 (2015) 43695–43704, https://doi.org/10.1039/C5RA02247A.
[27] P. Lorazo, L.J. Lewis, M. Meunier, Short-pulse laser ablation of solids: from phase explosion to fragmentation, Phys. Rev. Lett. 91 (2003) 225502, https://doi.org/10.1103/PhysRevLett.91.225502.
[28] B. Jung, P. Satish, D.N. Bunck, W.R. Dichtel, C.K. Ober, M.O. Thompson, Laser-induced sub-millisecond heating reveals distinct tertiary ester cleavage reaction pathways in a photolithographic resist polymer, ACS Nano 8 (2014) 5746–5756, https://doi.org/10.1021/nn500549w.
[29] X. Zang, C. Shen, Y. Chu, B. Li, M. Wei, J. Zhong, M. Sanghadasa, L. Lin, Laser-induced molybdenum carbide-graphene composites for 3D foldable paper electronics, Adv. Mater. 30 (2018) 1800062, https://doi.org/10.1002/adma.201800062.
[30] X. Zang, C. Jian, T. Zhu, Z. Fan, W. Wang, M. Wei, B. Li, M. Follmar Diaz, P. Ashby, Z. Lu, Y. Chu, Z. Wang, X. Ding, Y. Xie, J. Chen, J.N. Hohman, M. Sanghadasa, J.C. Grossman, L. Lin, Laser-sculptured ultrathin transition metal carbide layers for energy storage and energy harvesting applications, Nat. Commun. 10 (2019) 3112, https://doi.org/10.1038/s41467-019-10999-z.
[31] S.C. Rismiller, M.M. Groves, M. Meng, Y. Dong, J. Lin, Water assisted liquefaction of lignocellulose biomass by ReaxFF based molecular dynamic simulations, Fuel 215 (2018) 835–843, https://doi.org/10.1016/J.FUEL.2017.11.108.
[32] S. Shabnam, Q. Mao, A.C.T. van Duin, K.H. Luo, Evaluation of the effect of nickel clusters on the formation of incipient soot particles from polycyclic aromatic hydrocarbons *via* ReaxFF molecular dynamics simulations, Phys. Chem. Chem. Phys. 21 (2019) 9865–9875, https://doi.org/10.1039/C9CP00354A.
[33] C. Ashraf, S. Shabnam, A. Jain, Y. Xuan, A.C.T. van Duin, Pyrolysis of binary fuel mixtures at supercritical conditions: a ReaxFF molecular dynamics study, Fuel 235 (2019) 194–207, https://doi.org/10.1016/J.FUEL.2018.07.077.
[34] M. Kowalik, C. Ashraf, B. Damirchi, D. Akbarian, S. Rajabpour, A.C.T. van Duin, Atomistic scale Analysis of the carbonization process for C/H/O/N-based polymers with the ReaxFF reactive force field, J. Phys. Chem. B 123 (2019) 5357–5367, https://doi.org/10.1021/acs.jpcb.9b04298.
[35] J.R. Kershaw, K.J.T. Black, Structural characterization of coal-tar and petroleum pitches, Energy Fuel. 7 (1993) 420–425, https://doi.org/10.1021/ef00039a014.
[36] W.G. Hoover, Canonical dynamics: equilibrium phase-space distributions, Phys. Rev. A 31 (1985) 1695–1697, https://doi.org/10.1103/PhysRevA.31.1695.
[37] S. Nosé, A unified formulation of the constant temperature molecular dynamics methods, J. Chem. Phys. 81 (1984) 511–519, https://doi.org/10.1063/1.447334.
[38] MedeA-2.22, Materials Design, Inc, San Diego, CA, USA, 2018 n.d.
[39] R.W. Hockney, J.W. Eastwood, Computer Simulation Using Particles, A. Hilger, 1988. https://dl.acm.org/citation.cfm?id=62815. (Accessed 27 March 2019).
[40] G.-Y. Li, Q.-A. Xie, H. Zhang, R. Guo, F. Wang, Y.-H. Liang, Pyrolysis mechanism of metal-ion-exchanged lignite: a combined reactive force field and density functional theory study, Energy Fuel. 28 (2014) 5373–5381, https://doi.org/10.1021/ef501156b.
[41] S. Plimpton, Fast parallel algorithms for short-range molecular dynamics, J. Comput. Phys. 117 (1995) 1–19, https://doi.org/10.1006/JCPH.1995.1039.
[42] W. Humphrey, A. Dalke, K. Schulten, VMD: visual molecular dynamics, J. Mol. Graph. 14 (1996) 33–38. http://www.scopus.com/inward/record.url?eid=2-s2.0-0029878720&partnerID=40&md5=f5839d082c2c3b0cf4d1ae45bb39c3f8.
[43] A. Stukowski, Visualization and analysis of atomistic simulation data with OVITO–the Open Visualization Tool, Model. Simul. Mater. Sci. Eng. 18 (2010), https://doi.org/10.1088/0965-0393/18/1/015012, 015012.
[44] M. Zheng, X. Li, J. Liu, L. Guo, Initial chemical reaction simulation of coal pyrolysis via ReaxFF molecular dynamics, Energy Fuel. 27 (2013) 2942–2951, https://doi.org/10.1021/ef400143z.
[45] K. Fujiwara, A. Harada, J. Aihara, CH bond dissociation energies of polycyclic aromatic hydrocarbon molecular cations: theoretical interpretation of the (M-1)+ peak in the mass spectra, J. Mass Spectrom. 31 (1996) 1216–1220,

https://doi.org/10.1002/(SICI)1096-9888(199611)31:11<1216::AID-JMS409>3.0.CO;2-M.
[46] H. Wang, Formation of nascent soot and other condensed-phase materials in flames, Proc. Combust. Inst. 33 (2011) 41–67, https://doi.org/10.1016/J.PROCI.2010.09.009.
[47] B. Saha, S. Shindo, S. Irle, K. Morokuma, Simulations of dynamic fullerene self-assembly in benzene combustion, ACS Nano 3 (2009) 2241–2257.
[48] H.J. Qian, A.C.T. Van Duin, K. Morokuma, S. Irle, Reactive molecular dynamics simulation of fullerene combustion synthesis: ReaxFF vs DFTB potentials, J. Chem. Theory Comput. 7 (2011) 2040–2048, https://doi.org/10.1021/ct200197v.
[49] R.A. Causey, T.S. Elleman, K. Verghese, Hydrogen diffusion and solubility in pyrolytic carbon, Carbon 17 (1979) 323–328, https://doi.org/10.1016/0008-6223(79)90003-4.
[50] B. Saha, S. Irle, K. Morokuma, Formation mechanism of polycyclic aromatic hydrocarbons in benzene combustion: quantum chemical molecular dynamics simulations, J. Chem. Phys. 132 (2010), https://doi.org/10.1063/1.3447895, 224303.
[51] H. Takehara, M. Fujiwara, M. Arikawa, M.D. Diener, J.M. Alford, Experimental study of industrial scale fullerene production by combustion synthesis, Carbon 43 (2005) 311–319, https://doi.org/10.1016/J.CARBON.2004.09.017.
[52] R. Whitesides, M. Frenklach, Detailed kinetic Monte Carlo simulations of graphene-edge growth, J. Phys. Chem. A 114 (2010) 689–703, https://doi.org/10.1021/jp906541a.
[53] K. Fukui, T. Yonezawa, H. Shingu, A molecular orbital theory of reactivity in aromatic hydrocarbons, J. Chem. Phys. 20 (1952) 722–725, https://doi.org/10.1063/1.1700523.